PROCEEDINGS OF SCIENCE

Quantum simulation of entanglement and hadronization in high-energy collisions: lessons from the massive Schwinger model

Adrien Florio,[a,b] **David Frenklakh,**[a,c] **Kazuki Ikeda,**[b,c] **Dmitri Kharzeev,**[a,b,c] **Vladimir Korepin,**[b,d] **Shuzhe Shi**[e,*] **and Kwangmin Yu**[f]

[a] *Department of Physics, Brookhaven National Laboratory, Upton, New York 11973-5000, USA.*

[b] *Co-design Center for Quantum Advantage.*

[c] *Center for Nuclear Theory, Department of Physics and Astronomy, Stony Brook University, Stony Brook, New York 11794-3800, USA.*

[d] *C.N. Yang Institute for Theoretical Physics, Stony Brook University, Stony Brook, New York, 11794-3840, USA.*

[e] *Department of Physics, Tsinghua University, Beijing 100084, China.*

[f] *Computational Science Initiative, Brookhaven National Laboratory, Upton, New York 11973-5000, USA.*

E-mail: aflorio@bnl.gov, david.frenklakh@stonybrook.edu, kazuki.ikeda@stonybrook.edu, dmitri.kharzeev@stonybrook.edu, vladimir.korepin@stonybrook.edu, shuzhe-shi@tsinghua.edu.cn, kyu@bnl.gov

In this work, we investigate the potential connection between entanglement and thermalization, as well as the dynamics of hadronization in QCD physics. Through simulations of quantum dynamics on classical hardware, we analyze the real-time response of the massive Schwinger model coupled to external sources, which serves as an analog for the production and fragmentation of quark jets. This analogy is justified by the shared properties of confinement and chiral symmetry breaking between the Schwinger model and QCD. We observe the growth of time-dependent entanglement between the produced jets, which is driven by the increasing number of contributing eigenstates of the reduced density matrix with sufficiently large and closely spaced eigenvalues. This growth is intrinsically linked to the process of thermalization. The emergent eigenstates are identified as meson-like bound states, and by tracking their temporal evolution, we are able to observe real-time hadronization. At mid-rapidity, the long-time values of local observables approach approximately constant values, indicating the onset of equilibrium and the approach to thermalization.

The XVIth Quark Confinement and the Hadron Spectrum Conference (QCHSC24)
19-24 August, 2024
Cairns Convention Centre, Cairns, Queensland, Australia

*Speaker

 ISSN 1824-8039 . Published by SISSA Medialab.

PoS(QCHSC24)056

1. Introduction

The role of quantum entanglement in high-energy hadronic interactions has recently garnered significant interest [1–12]. Particularly, it has been found that QCD evolution generates a maximally entangled state (MES) at large rapidity separation y (or, equivalently, at small Bjorken $x = e^{-y}$) [1]. This MES contains a large number of microstates with n partons that possess approximately equal probabilities $p_n = p_n(y)$, giving rise to a maximal value of the entanglement entropy (EE)

$$S_E(y) = -\sum_n p_n \ln p_n. \tag{1}$$

The EE naturally emerges at high energies because the phase of the hadron wave function cannot be determined during the short Lorentz-contracted time of the interaction, so the measured density matrix corresponds to that of a pure hadron state traced over the unobserved phases [5].

If one assumes that hadron multiplicity distribution mirrors the distribution in the number of partons measured at a given rapidity, which is a stronger form of the "local parton-hadron duality" [13, 14], one may further postulate that the von Neumann entropy of the final hadron state S_H is equal to the entanglement entropy (1) [1–3]:

$$S_E = S_H. \tag{2}$$

Under this assumption, we get a relation between the soft gluon dominated parton structure function $x\,G(x) = \bar{n} = \sum_n n\, p_n$ and the entropy of hadronic final state that should hold for a MES [1], which has $p_n = \mathcal{N}^{-1}$ (with $\mathcal{N}$ being the maximal number of partons):

$$S_H = \ln \mathcal{N} = 2 \ln \big(x\,G(x)\big). \tag{3}$$

This relation is directly testable in experiments [2–4].

There is growing experimental evidence from deep inelastic scattering and high energy hadron interactions supporting the validity of the relation (3) [2, 4, 7, 15]. While the validity of (3) imposed by the emergence of MES is intriguing, there remain unanswered questions. First is the physics nature of the eigenstates of the reduced density matrix (known as Schmidt states). It has been conjectured that they correspond to parton states, but this conjectures remains unproven. Second, emergence of MES have not beed theoretically demonstrated in models with confinement (e.g., the treatment in [1] is based on Balitsky–Fadin–Kuraev–Lipatov (BFKL) dynamics that is conformally invariant). Third, there is compelling experimental evidence suggesting apparent thermalization in high-energy collisions – for example, hadron abundances can be described as thermal, with a universal effective temperature (see, e.g., [16, 17]). Whether this apparent thermalization a consequence of the emergence of a MES and whether there is a connection between the effective temperature and the confinement scale remain unknown.

Addressing these questions calls for a well-defined field theory model that shares key properties with QCD, such as confinement and chiral symmetry breaking, and allows for the treatment of real-time evolution at high energies from first principles, whether through analytical or numerical methods. In this work [18, 19] presented in the current proceeding, we tackle this challenge by employing a massive Schwinger model coupled to external sources. This framework mimics the production of high-energy back-to-back jets in QCD, as previously studied in [20–23]. Although the

massive Schwinger model cannot be solved analytically, it has been successfully investigated using quantum simulations (see [24, 25] for recent reviews) on both quantum [26–28] and classical [18, 29–36] hardware.

Our real-time simulations require the quantum circuit depth that exceeds the capabilities of the current quantum computers. While the quantum simulations on quantum computers using our approach should become possible in the near future (see for instance [27, 28]), in this work we use quantum simulations on classical hardware — we will complete exact diagonalization simulations on small lattices with tensor network simulations on larger lattices.

2. Quantum simulation of massive Schwinger model

To mimic the high energy collisions, we study the massive Schwinger model that couples to an external source that consists of a fermion and antifermion pair starting at the center of the lattice and going back-to-back along the lightcone, which was suggested in 1974 by Casher, Kogut, and Susskind [20]. As these external charges separate, the electric field between them is screened by dynamical fermion-antifermion pair production. Using open-boundary conditions, one is allowed to express the electric field only in terms of fermionic operators by solving Gauss' law, see for instance [37] for explicit expressions. Using staggered fermions, our time-dependent Hamiltonian reads (see [18] for more details)

$$H(t) = -\frac{i}{2a}\sum_{n=1}^{N-1}\left(\chi_n^\dagger \chi_{n+1} - \chi_{n+1}^\dagger \chi_n\right) + m\sum_{n=1}^{N}(-1)^n \chi_n^\dagger \chi_n + \frac{ag^2}{2}\sum_{n=1}^{N-1}\left(L_{\mathrm{dyn},n} + L_{\mathrm{ext},n}(t)\right)^2 , \quad (4)$$

where n labels lattice sites, going from 1 to the length of the lattice N; $\chi_n^\dagger$ are fermionic creation operators, m, g, and a are the fermion mass, electric charge, and lattice spacing, respectively. In the last term we use

$$L_{\mathrm{dyn},n} = \sum_{i=1}^{n} q_i \,, \qquad L_{\mathrm{ext},n}(t) = -\theta\left(\frac{t-t_0}{a} - \left|n - \frac{N}{2}\right|\right) , \quad (5)$$

where the first equation defines the dynamical lattice electric field operator in terms of the local charge operators $q_i = \chi_i^\dagger \chi_i + \frac{(-1)^i - 1}{2}$. The second equation describes the electric field due to the external sources propagating back to back along the lightcone.

To study jet propagation in the vacuum, we begin the simulation in the vacuum state $|\Psi_0\rangle$ of the massive Schwinger model without the external source, described by the Hamiltonian $H(t = 0)$. The subsequent time evolution of this state is determined by the full Hamiltonian including the external source:

$$|\Psi_t\rangle = \mathcal{T} e^{-i\int_0^t dt' H(t')} |\Psi_0\rangle, \quad (6)$$

where $\mathcal{T}$ denotes time ordering. We perform the time evolution numerically using exact diagonalization for small lattice ($N \leq 20$), as well as tensor networks methods for larger ones ($20 < N \leq 100$). In more detail, the Density Matrix Renormalization Group (DMRG) is used to find a Matrix Product State (MPS) approximation of the ground state, which is subsequently evolved using the Time-Dependent Varational Principle (TDVP). We use the open-source ITensors library [52] as our primary software source. Exact diagonalization preserves the full information about the state

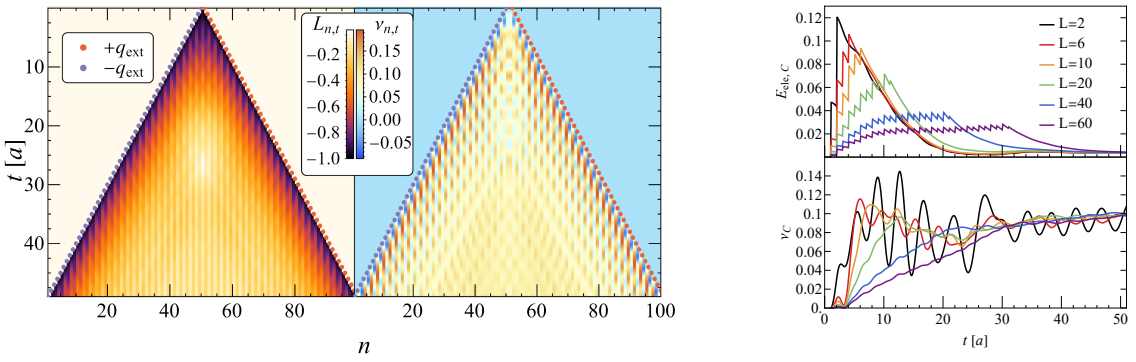

Figure 1: Left: The distribution of electric field (left) and local fermion condensate (right, c.f. Eq.7) as a function of space and time. The vacuum values are subtracted. Red and blue circles denote the positions of the external positive and negative charge respectively at the corresponding time. **Right**: averaged electric field energy $E_{\text{ele, C}}(L) = \frac{1}{L}\frac{ag^2}{2}\sum_{n=N/2-L/2+1}^{N/2+L/2}(L_{\text{dyn},n} + L_{\text{ext},n}(t))^2$ (upper) and fermion condensate (lower, c.f. Eq.8), modulo their vacuum values. In both of plots, the system parameters are $m = 1/(4a), g = 1/(2a), N = 100$.

(6) and allows to extract any quantity characterizing the quantum state. Tensor networks allow to simulate much larger systems and surprisingly long-time evolution. Note that time evolution continues until external charges reach the edges of the lattice at $t = \frac{aN}{2}$ and then the simulation stops.

The propagating jets can modify the nonperturbative structure of the vacuum. We quantify this modification by measuring the local scalar fermion density $\langle\bar{\psi}\psi\rangle$ that is known to have a negative value in the vacuum of the Schwinger model. On the lattice it is related to the local charge density as:

$$\nu_{n,t} \equiv \frac{(-1)^n}{a} q_n - \frac{1}{2a}. \tag{7}$$

In the presence of external sources this local condensate deviates from its vacuum value due to jet propagation. This deviation as a function of both space and time for $N = 100$, $m = \frac{1}{4a}$, $g = \frac{1}{2a}$ is shown in Fig. 1 (left). As one can see, the condensate disruption closely follows the propagating jets. At late times the value of the condensate settles to a nearly constant value (different from the vacuum one) in the central region. To see how exactly this relaxation to a new value happens, we average the deviation of the condensate from its vacuum value over a region of size L in the center of the system:

$$\nu_C(L) \equiv \frac{1}{L}\sum_{n=N/2-L/2+1}^{N/2+L/2}(\nu_{n,t} - \nu_{n,0}). \tag{8}$$

In Fig. 1 (right), we show $\nu_C(L)$ as a function of time for a few different values of the central region size. We find that at sufficiently late times the average value of the condensate reaches the same constant value regardless of the size of the region where averaging is performed. This signals a step towards some equilibrium value induced by the jets in the central part of the system. Analogous behavior is observed for the electric field and the electric energy, both of which tends to

be fully screened. Whether or not these equilibrium values correspond to the thermal equilibrium needs a detailed analysis of the entropy that follows.

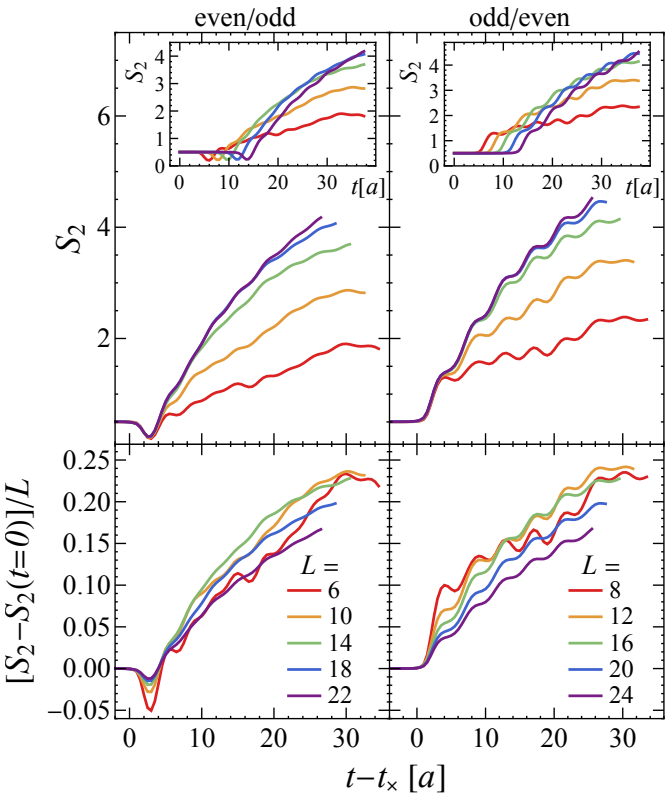

Figure 2: Top panel: second Rényi entropy as a function of $t - t_\times$, with $t_\times$ the time at which the external sources cross the boundaries of the sublattice, for different sublattice in the center. The left(right) panels correspond to odd sites-even sites(even sites-odd sites) boundaries. They differ because of the staggering, which is a lattice artifact. **Bottom panel**: substracted second Renyi entropy rescaled by the size of the sublattice as a function of $t - t_\times$ for different sublattice in the center. Smaller subsystems start exhibiting volume law at a late time, exhibited by the fact the saturate to the same value on this plot. The left and right panels correspond to odd sites- even sites and even sites-odd sites boundaries, respectively. **Insets**: the corresponding second Renyi entropy as a function of time.

While the entropy of a pure state wave function (6) is aways zero, themalization could take place in a sublattice. In the context of thermodynamics, a sublattice is a subsystem in thermal and chemical contact with a reservoir. Thus, for a sublattice with length L, one may compute the reduced density matrix by tracing out the complementary set (reservoir), $\rho_L(t) = \mathrm{tr}_{\bar{L}}(|\Psi_t\rangle\langle\Psi_t|)$, and the entropy can be estimated from the Rényi entropy:

$$S_\alpha(t) \equiv \frac{\ln \mathrm{Tr}_L(\rho_L(t)^\alpha)}{1-\alpha}, \tag{9}$$

which resembles the definition of von Neumann entropy when its order (α) approaches unity. The time-dependence of Rényi entropies for several different values of L is shown in Fig. 2. For readability, we separated the cases with $L/2$ odd (corresponding to even and odd sites at the boundary) and even (corresponding to odd and even sites at the boundary). While this distinction is irrelevant in the continuum limit, the staggering induces quantitative differences. The qualitative features, on the other hand, are the same. As soon as the external particles cross the boundaries of the subsystem ($t = t_\times = L/2$) the Rényi entropies start growing. Initially, the growth is independent of the subsystem size; the state still follows an area law. After some time which grows with the subsystem size, the value of the entanglement entropy starts depending on the subsystem size, before eventually reaching a plateau (in the present simulation the plateau is reached only for $L \in [6, 16]$).

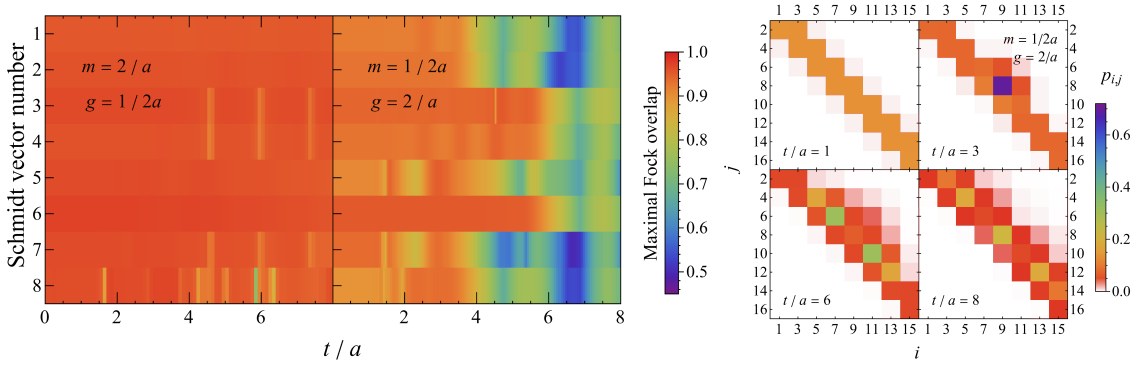

Figure 3: Left: Maximal overlap of each Schmidt vector with any Fock state. Comparison between $m = 2/a, g = 1/(2a)$ on the left panel and $m = 1/(2a), g = 2/a$ on the right panel is shown. In both cases, $N = 16$. To study continuous evolution, we choose to consider the 8 leading Schmidt vectors in the vacuum state at $t = 0$ and follow their evolution. Because of the level crossing in Schmidt spectrum, at later times these vectors are not necessarily the 8 leading Schmidt vectors. **Right**: One-pair overlaps for $N = 16$, $m = 1/(2a), g = 2/a$ for the select moments of time evolution from $t = a$ to $t = 8a$. Color denotes the magnitude of overlap with the one-pair excitation that creates the i^{th} antifermion and j^{th} fermion from the Néel state, $p_{ij} = |\langle\Psi_t|\chi_i\chi_j^\dagger|\mathcal{N}\rangle|$ while the horizontal and vertical directions on the grid span i and j, respectively.

Moreover, the leading dependence on the system size is linear once the plateau is reached. This is demonstrated in the lower panel of Fig.2, where we show the value of the Rényi entropy with the vacuum value subtracted, divided by the subsystem size. In other words, the system transitions from following the area law to the volume law of entanglement.

We note that, even if in a different setup, the observed behavior is reminiscent of the typical response of many-body ground states to global quenches. There, subsystems in finite volumes follow an area law as a function for a finite time t_a, before transitioning to a volume law once relaxed. Moreover, at early time $t < t_a$, the value of the entanglement entropy is often seen to grow linearly as a function of time (irrespectively of the subsystem size, as a consequence of the area law) [38]. This seems also to be the case in our setup.

Analyses of condensate density, electric field, and entropy, support that excitations induced by a high-energy collisions are thermalizing. Then a natural questions, what is the physical nature of these excitations? To address this question, we analyze the physical meaning of the states contributing to the entropy of the reduced density matrix:

$$\rho_L(t) = \sum_j \lambda_j(t)|\psi_j^L(t)\rangle\langle\psi_j^L(t)|. \tag{10}$$

Here, $|\psi_j^L\rangle$'s are referred to as the Schmidt basis, to which we have direct access with exact diagonalization. In order to elucidate the relationship between the Schmidt vectors and partonic states (with the fundamental fermions of the Schwinger model playing the role of partons) we compare the properties of the Schmidt vectors in two regimes of the theory: at weak coupling and at strong coupling. Throughout this section we study the system with lattice size $N = 16$ and two sets of mass and the coupling constant: i) $m = 2/a$, $g = 1/(2a)$ and ii) $m = 1/(2a)$, $g = 2/a$.

At infinite fermion mass m and in the occupation number basis, the vacuum state of our system is the so-called Néel state: $|\mathcal{N}\rangle = |1010\ldots10\rangle$ (which translates into unoccupied fermion and antifermion sites). The Néel state is a useful zeroth approximation to the true vacuum state even for the finite values of the fermion mass used in this study. Deviations from the Néel state can be classified according to which pairs of sites (one for fermion and another one for antifermion) are "excited" with respect to the Néel state. The simplest example is given by "one-pair" excitations $|ij\rangle = \chi_i\chi_j^\dagger|\mathcal{N}\rangle$, where i is odd and j is even. In the large mass and infinite volume limits $|ij\rangle$ would be the $(N^2/4)$-fold degenerate first excited states above the vacuum Néel state. Note that a single excitation is prohibited in the charge-zero sector. Since the ground state is in this sector and the Hamiltonian evolution conserves the total charge, the state (6) is always at the charge-zero sector. All possible excitations form a basis which we will refer to as the Fock basis.

Each of the Schmidt vectors can also be decomposed in the Fock basis on half of the lattice. In this case Fock states are not restricted to the charge-zero sector, but have the same charge as the corresponding Schmidt vector. For each Schmidt vector, let us concentrate on the Fock state with which it has the largest overlap. In Fig. 3 the time evolution of this maximal overlap for the 8 leading Schmidt vectors is shown in weak coupling and strong coupling regimes. At weak coupling (Fig. 3, left) the overlap stays close to 1 at all times, signaling that the Schmidt vectors are very close to the partonic Fock states. On the other hand, at strong coupling (Fig. 3, mid) this overlap is also large in the vacuum state ($t = 0$) but decreases during the time evolution. This is a manifestation of hadronization in real time: at first the system is described by partonic (fermionic) degrees of freedom but with jet fragmentation the relevant degrees of freedom become bosonic.

Finally, in Fig. 3 (right) we visualize the full quantum state evolution by calculating the probability of finding the system in one of the one-pair states. In the initial state all the nearest-neighbor pairs are excited almost equally, modulo the small boundary effects. In the subsequent evolution the excitation above the vacuum state spreads along the lightcone. At strong coupling some next-to-nearest-neighbor pairs get substantially excited later in the evolution, while still following the lightcone propagation. This effect demonstrates that the excitations at strong coupling and smaller fermion mass are no longer localized. Moreover, the pairs of a certain orientation ($i > j$) are strongly preferred at later times. These are the states that screen the external electric field inside them.

3. Summary and Discussions

In the studies [18, 19] presented in this proceeding, we explored the growth of entanglement and the thermalization process of propagating jets in the 1 + 1-dimensional massive Schwinger model. By analyzing the symmetry-resolved half-lattice Schmidt spectrum, we enhanced our understanding of entanglement generation in the system. These findings, combined with exact diagonalization, provided a qualitative insight into the asymptotic states of the theory.

We noted that the central rapidity region of our system reaches a steady state at late times, which is independent of the subsystem's size. This implies that particle production drives thermalization. While a definitive assessment requires comparing all properties of this steady state to thermal ensembles—a task reserved for future research—the thermalization hypothesis is further supported by the behavior of entanglement. By calculating the second Rényi entropy over central regions,

we observed a clear transition from the area law to the volume law for entanglement, essential for achieving an extensive thermodynamical entropy. We concluded our analysis by measuring the information propagation speed, confirming it saturates at the speed of light.

Additionally, we examined the nature of asymptotic states contributing to the entanglement entropy as a function of coupling. At weak coupling, these states closely resemble partonic Fock states. Conversely, at strong coupling, the overlap between Schmidt states and partonic states diminishes over time, likely indicating a transition toward bosonic Fock states. In essence, we directly observed, in real-time, the equivalent of hadronization in the massive Schwinger model.

With direct experimental measurements of entanglement becoming feasible, not only in deep-inelastic scattering [3] but also in high-energy proton-proton collisions (e.g., recent ATLAS collaboration measurements [39]), advancing first-principle, real-time investigations of entanglement structure and dynamics in relativistic field theory is crucial. This work represents a step in that direction, opening exciting avenues for future research. One key direction is to characterize thermalization more precisely. Specifically, since the system is closed and evolves as a pure state, apparent thermalization aligns with the Eigenstate Thermalization Hypothesis (ETH), a cornerstone of quantum thermalization in many-body physics (see e.g., [40]). However, ETH applies to finite-size systems. Clarifying this relationship or extending ETH to this dynamical context would bridge the growing literature on thermalization in gauge theory from a quantum dynamics perspective (e.g., [41–49]). The connection to many-body physics and quantum information theory also introduces other intriguing quantities to explore, such as information scrambling in this model, which is expected to relate to the saturation time of the second Rényi entropy [50], and the behavior of mixed-state entanglement [51].

In summary, we have investigated the real-time behavior of entanglement entropy and the entanglement spectrum in the massive Schwinger model coupled to external sources—a setup analogous to jet production in high-energy QCD. Our findings offer valuable insights into the microscopic dynamics of hadronization and thermalization in confining quantum field theories, paving the way for new theoretical and experimental explorations.

Acknowledgement

We thank Yuri Dokshitzer, Andreas Elben, Swagato Mukherjee, Anatoli Polkovnikov, Mark Srednicki, and Torsten Zache for useful discussions and communications. We acknowledge valuable discussions at the workshop “Thermalization, from Cold Atoms to Hot Quantum Chromodynamics" that was held during September 2023 at the InQubator for Quantum Simulation (IQuS) hosted by the Institute for Nuclear Theory (INT). The InQubator for Quantum Simulation is supported by U.S. Department of Energy, Office of Science, Office of Nuclear Physics, InQubator for Quantum Simulation (IQuS) under Award Number DOE (NP) Award DE-SC0020970 via the program on Quantum Horizons: QIS Research and Innovation for Nuclear Science. This work was supported by the U.S. Department of Energy, Office of Science, National Quantum Information Science Research Centers, Co-design Center for Quantum Advantage (C2QA) under Contract No.DE-SC0012704 (AF, KI, DK, VK), the U.S. Department of Energy, Office of Science, Office of Nuclear Physics, Grants Nos. DE-FG88ER41450 (DF, DK) and DE-SC0012704 (AF, DK, KY), and Tsinghua University under grant No. 53330500923 (SS). This research used resources of the National Energy

Research Scientific Computing Center, a DOE Office of Science User Facility supported by the Office of Science of the U.S. Department of Energy under Contract No. DE-AC02-05CH11231 using NERSC award NERSC DDR-ERCAP0028999.

References

[1] D. E. Kharzeev and E. M. Levin, Phys. Rev. D **95** (2017) no.11, 114008, [arXiv:1702.03489 [hep-ph]].

[2] Z. Tu, D. E. Kharzeev and T. Ullrich, Phys. Rev. Lett. **124** (2020) no.6, 062001, [arXiv:1904.11974 [hep-ph]].

[3] M. Hentschinski, D. E. Kharzeev, K. Kutak and Z. Tu, Phys. Rev. Lett. **131** (2023) no.24, 241901, [arXiv:2305.03069 [hep-ph]].

[4] V. Andreev *et al.* [H1], Eur. Phys. J. C **81** (2021) no.3, 212, [arXiv:2011.01812 [hep-ex]].

[5] D. E. Kharzeev, Phil. Trans. A. Math. Phys. Eng. Sci. **380** (2021) no.2216, 20210063, [arXiv:2108.08792 [hep-ph]].

[6] N. Armesto, F. Dominguez, A. Kovner, M. Lublinsky and V. Skokov, JHEP **05** (2019), 025, [arXiv:1901.08080 [hep-ph]].

[7] D. E. Kharzeev and E. Levin, Phys. Rev. D **104** (2021) no.3, L031503, [arXiv:2102.09773 [hep-ph]].

[8] G. Dvali and R. Venugopalan, Phys. Rev. D **105** (2022) no.5, 056026, [arXiv:2106.11989 [hep-th]].

[9] K. Zhang, K. Hao, D. Kharzeev and V. Korepin, Phys. Rev. D **105** (2022) no.1, 014002, [arXiv:2110.04881 [quant-ph]].

[10] Y. Liu, M. A. Nowak and I. Zahed, Phys. Rev. D **105** (2022) no.11, 114027, [arXiv:2202.02612 [hep-ph]].

[11] Y. Liu, M. A. Nowak and I. Zahed, Phys. Rev. D **105** (2022) no.11, 114028, [arXiv:2203.00739 [hep-ph]].

[12] A. Dumitru, A. Kovner and V. V. Skokov, Phys. Rev. D **108** (2023) no.1, 014014, [arXiv:2304.08564 [hep-ph]].

[13] Y. I. Azimov, Y. L. Dokshitzer, V. A. Khoze and S. I. Troyan, Z. Phys. C **27** (1985), 65-72,

[14] Y. L. Dokshitzer, V. A. Khoze and S. I. Troian, J. Phys. G **17** (1991), 1585-1587,

[15] M. Hentschinski and K. Kutak, Eur. Phys. J. C **82** (2022) no.2, 111 [erratum: Eur. Phys. J. C **83** (2023) no.12, 1147], [arXiv:2110.06156 [hep-ph]].

[16] F. Becattini and U. W. Heinz, Z. Phys. C **76** (1997), 269-286 [erratum: Z. Phys. C **76** (1997), 578], [arXiv:hep-ph/9702274 [hep-ph]].

[17] A. Andronic, P. Braun-Munzinger and J. Stachel, Phys. Lett. B **673** (2009), 142-145 [erratum: Phys. Lett. B **678** (2009), 516], [arXiv:0812.1186 [nucl-th]].

[18] A. Florio, D. Frenklakh, K. Ikeda, D. Kharzeev, V. Korepin, S. Shi and K. Yu, Phys. Rev. Lett. **131** (2023) no.2, 021902, [arXiv:2301.11991 [hep-ph]].

[19] A. Florio, D. Frenklakh, K. Ikeda, D. E. Kharzeev, V. Korepin, S. Shi and K. Yu, Phys. Rev. D **110** (2024) no.9, 094029, [arXiv:2404.00087 [hep-ph]].

[20] A. Casher, J. B. Kogut and L. Susskind, Phys. Rev. D **10** (1974), 732-745.

[21] F. Loshaj and D. E. Kharzeev, Int. J. Mod. Phys. E **21** (2012), 1250088, [arXiv:1111.0493 [hep-ph]].

[22] D. E. Kharzeev and F. Loshaj, Phys. Rev. D **87** (2013) no.7, 077501, [arXiv:1212.5857 [hep-ph]].

[23] D. E. Kharzeev and F. Loshaj, Phys. Rev. D **89** (2014) no.7, 074053, [arXiv:1308.2716 [hep-ph]].

[24] C. W. Bauer, Z. Davoudi, A. B. Balantekin, T. Bhattacharya, M. Carena, W. A. de Jong, P. Draper, A. El-Khadra, N. Gemelke and M. Hanada, *et al.* PRX Quantum **4** (2023) no.2, 027001, [arXiv:2204.03381 [quant-ph]].

[25] C. W. Bauer, Z. Davoudi, N. Klco and M. J. Savage, Nature Rev. Phys. **5** (2023) no.7, 420-432, [arXiv:2404.06298 [hep-ph]].

[26] N. Klco, E. F. Dumitrescu, A. J. McCaskey, T. D. Morris, R. C. Pooser, M. Sanz, E. Solano, P. Lougovski and M. J. Savage, Phys. Rev. A **98** (2018) no.3, 032331, [arXiv:1803.03326 [quant-ph]].

[27] R. C. Farrell, M. Illa, A. N. Ciavarella and M. J. Savage, PRX Quantum **5** (2024) no.2, 2, [arXiv:2308.04481 [quant-ph]].

[28] R. C. Farrell, M. Illa, A. N. Ciavarella and M. J. Savage, Phys. Rev. D **109** (2024) no.11, 11, [arXiv:2401.08044 [quant-ph]].

[29] T. V. Zache, N. Mueller, J. T. Schneider, F. Jendrzejewski, J. Berges and P. Hauke, Phys. Rev. Lett. **122** (2019) no.5, 050403, [arXiv:1808.07885 [quant-ph]].

[30] M. Rigobello, S. Notarnicola, G. Magnifico and S. Montangero, Phys. Rev. D **104** (2021) no.11, 114501, [arXiv:2105.03445 [hep-lat]].

[31] W. A. de Jong, K. Lee, J. Mulligan, M. Płoskoń, F. Ringer and X. Yao, Phys. Rev. D **106** (2022) no.5, 054508, [arXiv:2106.08394 [quant-ph]].

[32] R. Belyansky, S. Whitsitt, N. Mueller, A. Fahimniya, E. R. Bennewitz, Z. Davoudi and A. V. Gorshkov, Phys. Rev. Lett. **132** (2024) no.9, 091903, [arXiv:2307.02522 [quant-ph]].

[33] K. Ikeda, D. E. Kharzeev, R. Meyer and S. Shi, Phys. Rev. D **108** (2023) no.9, L091501, [arXiv:2305.00996 [hep-ph]].

[34] J. Barata, W. Gong and R. Venugopalan, Phys. Rev. D **109** (2024) no.11, 116003, [arXiv:2308.13596 [hep-ph]].

[35] K. Ikeda, D. E. Kharzeev and S. Shi, Phys. Rev. D **108** (2023) no.7, 074001, [arXiv:2305.05685 [hep-ph]].

[36] K. Lee, J. Mulligan, F. Ringer and X. Yao, Phys. Rev. D **108** (2023) no.9, 094518, [arXiv:2308.03878 [quant-ph]].

[37] K. Ikeda, D. E. Kharzeev and Y. Kikuchi, Phys. Rev. D **103** (2021) no.7, L071502, [arXiv:2012.02926 [hep-ph]].

[38] J. Eisert, M. Cramer and M. B. Plenio, Rev. Mod. Phys. **82** (2010), 277-306, [arXiv:0808.3773 [quant-ph]].

[39] G. Aad *et al.* [ATLAS], Nature **633** (2024) no.8030, 542-547, [arXiv:2311.07288 [hep-ex]].

[40] J. M. Deutsch, Rept. Prog. Phys. **81** (2018) no.8, 082001.

[41] D. Kharzeev and K. Tuchin, Nucl. Phys. A **753** (2005), 316-334, [arXiv:hep-ph/0501234 [hep-ph]].

[42] J. Berges, S. Floerchinger and R. Venugopalan, JHEP **04** (2018), 145, [arXiv:1712.09362 [hep-th]].

[43] Z. Y. Zhou, G. X. Su, J. C. Halimeh, R. Ott, H. Sun, P. Hauke, B. Yang, Z. S. Yuan, J. Berges and J. W. Pan, Science **377** (2022) no.6603, abl6277, [arXiv:2107.13563 [cond-mat.quant-gas]].

[44] N. Mueller, T. V. Zache and R. Ott, Phys. Rev. Lett. **129** (2022) no.1, 011601, [arXiv:2107.11416 [quant-ph]].

[45] J. Y. Desaules, D. Banerjee, A. Hudomal, Z. Papić, A. Sen and J. C. Halimeh, Phys. Rev. B **107** (2023) no.20, L201105, [arXiv:2203.08830 [cond-mat.str-el]].

[46] L. Ebner, B. Müller, A. Schäfer, C. Seidl and X. Yao, Phys. Rev. D **109** (2024) no.1, 014504, [arXiv:2308.16202 [hep-lat]].

[47] X. Yao, Phys. Rev. D **108** (2023) no.3, L031504, [arXiv:2303.14264 [hep-lat]].

[48] S. Grieninger, K. Ikeda, D. E. Kharzeev and I. Zahed, Phys. Rev. D **109** (2024) no.1, 016023, [arXiv:2312.03172 [hep-th]].

[49] S. Chen, L. Yan and S. Shi, [arXiv:2412.00662 [hep-ph]].

[50] Y. O. Nakagawa, M. Watanabe, S. Sugiura and H. Fujita, Nature Commun. **9** (2018) no.1, 1635, [arXiv:1703.02993 [cond-mat.stat-mech]].

[51] A. Florio, Phys. Rev. D **109** (2024) no.7, L071501, [arXiv:2312.05298 [hep-th]].

[52] M. Fishman, S. R. White and E. M. Stoudenmire, SciPost Phys. Codeb. **2022** (2022), 4, [arXiv:2007.14822 [cs.MS]].